REPORT DOCUMENTATION PAGE

Form Approved
OMB No. 0704-0188

1. REPORT DATE *(DD-MM-YYYY)*	2. REPORT TYPE	3. DATES COVERED *(From - To)*
August 2004	Technical Paper	August 2004

4. TITLE AND SUBTITLE
System Identification Methods for Improving Flutter Flight Test Techniques

5a. CONTRACT NUMBER

5b. GRANT NUMBER

5c. PROGRAM ELEMENT NUMBER

6. AUTHOR(S)
Klyde, David
Harris, Chuck

5d. PROJECT NUMBER

5e. TASK NUMBER

5f. WORK UNIT NUMBER

7. PERFORMING ORGANIZATION NAME(S) AND ADDRESS(ES) AND ADDRESS(ES)
412 TW/ENTT
Air Force Flight Test Center (AFFTC)
Edwards AFB, CA 93524

8. PERFORMING ORGANIZATION REPORT NUMBER
PA-04145

9. SPONSORING / MONITORING AGENCY NAME(S) AND ADDRESS(ES)
412 TW/ENTT
Air Force Flight Test Center (AFFTC)
Edwards AFB, CA 93524

10. SPONSOR/MONITOR'S ACRONYM(S)

11. SPONSOR/MONITOR'S REPORT NUMBER(S)
N/A

12. DISTRIBUTION / AVAILABILITY STATEMENT
A Approved for public release; distribution is unlimited.

20040922 005

13. SUPPLEMENTARY NOTES
CC: 012100 CA: Air Force Flight Test Center Edwards AFB

14. ABSTRACT
Classic flutter flight testing involves the evaluation of a given configuration at a stabilized test point before clearance is given to expand the envelope further. At each stabilized point flight test data are compared with computer simulation models to assess the accuracy of predicted flutter boundaries. Because of the time constraints associated with these procedures, the Air Force has been seeking methods to improve current flight test methods. This paper describes a technique that provides a rapid, on-line tool for the identification of aeroservoelastic (ASE) systems. The technique involves the use of discrete wavelet transforms to compute the impulse response (Markov parameters) of the estimated system. This is then used in the Eigensystem Realization Algorithm (ERA) method to compute the discretized state-space matrices. The technique used herein includes metrics that are used to assess the validity of the identified system. Although the method does require that the identification begin from stabilized initial conditions, it has been shown to be relatively insensitive to input forcing function. A model of a modern naval fighter aircraft was used to evaluate the capabilities of the identification method. The identification techniques were evaluated with and without an active oscillation controller in place.

15. SUBJECT TERMS
Aeroservoelastic (ASE) Limit cycle oscillation (LCO) Fast Fourier Transform (FFT) Active Flutter Suppression (AFS)
Discrete wavelet transform (DWT) Modal Amplitude Coherence (MAC) Mode Singular Value (MSV)
Eigensystem Realization Algorithm (ERA) Systems Technology, Inc. (STI) Active oscillation controller (AOC)

16. SECURITY CLASSIFICATION OF:			17. LIMITATION OF ABSTRACT	18. NUMBER OF PAGES	19a. NAME OF RESPONSIBLE PERSON
					Chuck Harris
a. REPORT	b. ABSTRACT	c. THIS PAGE	Unclassified Unlimited	14	19b. TELEPHONE NUMBER *(include area code)* 661-277-3737
UNCLASSIFIED	UNCLASSIFIED	UNCLASSIFIED			

SYSTEM IDENTIFICATION METHODS FOR IMPROVING FLUTTER FLIGHT TEST TECHNIQUES

Edward N. Bachelder
David H. Klyde
Peter M. Thompson
Systems Technology, Inc.
Hawthorne, CA

Chuck Harris
Air Force Flight Test Center
Edwards AFB, CA

ABSTRACT

Classic flutter flight testing involves the evaluation of a given configuration at a stabilized test point before clearance is given to expand the envelope further. At each stabilized point flight test data are compared with computer simulation models to assess the accuracy of predicted flutter boundaries. Because of the time constraints associated with these procedures, the Air Force has been seeking methods to improve current flight test methods. This paper describes a technique that provides a rapid, on-line tool for the identification of aeroservoelastic systems. The technique involves the use of discrete wavelet transforms to compute the impulse response (Markov parameters) of the estimated system. This is then used in the Eigensystem Realization Algorithm (ERA) method to compute the discretized state-space matrices. The technique used herein includes metrics that are used to assess the validity of the identified system. Although the method does require that the identification begin from stabilized initial conditions, it has been shown to be relatively insensitive to input forcing function. A model of a modern naval fighter aircraft was used to evaluate the capabilities of the identification method. The identification techniques were evaluated with and without an active oscillation controller in place.

INTRODUCTION

Under certain common loading configurations, the F-16C/D experiences a 5 Hz limit cycle oscillation (LCO) that involves an interaction of asymmetric wingtip pitching and store pitching modes (Ref. 1). This limited amplitude form of flutter is most commonly found in the 350 to 450 KCAS region. Although this form of flutter does not impact structural integrity, it can produce significant ride quality problems for the pilot. Lockheed Martin Tactical Aircraft Systems was contracted by the Air Force to develop and demonstrate a non-adaptive active flutter suppression system to reduce or eliminate this LCO phenomenon. The resulting control laws use the flaperons to counteract the motion of the 5 Hz LCO. Although the system was not successful at all flight conditions and loading configurations tested in flight, it did demonstrate a means for allowing an expanded flight envelope on an operational aircraft. According to Ref. 1 specific problems encountered in the flight test program included the requirement for a very detailed and complex test procedure to optimize AFS control gains. In addition, poor initial gain and phase predictions for the AFS were not well suited to suppress the LCO and the required gains changed quickly as the aircraft accelerated above Mach 0.9 to 0.95.

This program and other related work sponsored by the Air Force has emphasized a need for improved aeroservoelastic prediction models and flutter flight test techniques. In response to the need for improved models, significant research and development has been conducted by the University of Colorado at Boulder (Refs. 2 and 3). The approach taken is to use nonlinear methods that better capture the unsteady flow characteristics in the transonic region that features mixed subsonic-supersonic flow patterns. The

technique has been applied to stabilized, accelerated, and increased angle-of attack configurations. Systems Technology, Inc. has been contracted by the Air Force Flight Test Center to develop improved flutter flight test techniques for aircraft with and without a flutter suppression system. This work has led to the Wavelet-Eigensystem Realization Algorithm system identification method, among others, that is the focus of this paper.

THE WAVELET-ERA METHOD

A methodology has been developed that estimates the frequency response of a given system using an arbitrary input and the system's response. This technique uses the discrete wavelet transform as given in previous progress reports. However, if it can be assumed that the system is initially at rest (i.e., the aircraft is trimmed), then the technique is greatly simplified. When the initial conditions are zero, the system response consists entirely of a forced response from the time the input is first applied until the end of the data measurement. Thus it is not necessary to estimate what the system dynamics are, which would have been required for an estimate of the free response.

The discrete wavelet transform of the impulse response is computed using the forcing input and system response, and the inverse wavelet transform is then computed to produce the time-domain impulse response (also known as the Markov parameters). Finally, the Eigensystem Realization Algorithm (ERA) method is used to compute the discretized state-space matrices, from which is generated the magnitude and phase of the system response.

The experimental identification of physical vibration modes and mode shapes can be done with impulse response functions that are extracted from measured vibration records. In order to extract these impulse response functions, the Fast Fourier Transform (FFT) has often been used in conjunction with repeated data filtering and windowing (Ref. 4). These techniques require input signals that are rich enough to excite structural frequencies of interest – this does not appear to be the case with wavelet analysis. Moreover, with its more intuitive decomposition of data, wavelets analysis allows identification of time-varying system parameters.

The system realization, based on a first-order state space model, can be represented as:

$$\dot{x}(t) = Ax(t) + Bu(t)$$

$$y = Cx(t) + Du(t) \tag{1}$$

In the time domain, the solution at time t_n to Equation 1 can be expressed as:

$$y(t_n) = \int_{-\infty}^{n} h(t_n - \tau)u(\tau)d\tau \tag{2}$$

where h(t) is the temporal impulse response function. This convolution formula can be expressed in matrix form by:

$$Y = hU \tag{3}$$

In Equation 3, Y represents the output matrix, U is the input matrix, and h is the time-domain impulse response matrix. Once h is known the output of our system can be determined for any arbitrary input. An accurate extraction of h(t), often referred as the Markov parameters, will identify a system (Ref. 5) since

$$h(t) = Ce^{At}B$$

(4)

One could try to obtain h(t) directly by applying a unit impulse input u(t). In this case, y(t) would theoretically be identical to our desired h(t). However, this is practically unfeasible. Looking at Equation 3, if the input signals are not rich in frequency content, or the sampling size is too large, U can become ill-conditioned and the corresponding impulse response function cannot be computed accurately. Moreover, the computations associated with h(t) can be intensive. For these reasons, FFT-based extraction of the impulse response function is widely used (Ref. 4) since it has high computational efficiency and reasonable robustness provided the input data is rich in frequency content. However, if the input load u consists of only a single or a few frequencies, the temporal impulse response data tends to be erratic and badly conditioned. Wavelet analysis appears to offer a more robust alternative.

COMPUTATIONAL TECHNIQUE

Wavelet Theory

The wavelet transform allows any arbitrary signal $f(x)$ to be decomposed into an infinite summation of wavelets at different scales according to the expansion (Ref. 6):

$$f(x) = \sum_{j=-\infty}^{\infty} \sum_{k=-\infty}^{\infty} c_{j,k} W(2^j x - k)$$

(5)

The $W(2^j x-k)$ functions are the wavelets and provide a local basis along the time axis. To see how wavelets can be generated from the so-called dilation equation and their relation to the scaling functions $\varphi(x)$, the reader is directed to Ref. 7. Because of the way in which the wavelets are defined, when j is negative, the wavelets $W(2^j x-k)$ can be expressed as a sum of terms like $\varphi(x-k)$. The corresponding wavelet transform can then be expressed as follows:

$$f(x) = \sum_{k=-\infty}^{\infty} c_{\varphi,k} \varphi(x-k) + \sum_{j=0}^{\infty} \sum_{k=-\infty}^{\infty} c_{j,k} W(2^j x - k)$$

(6)

In this approach, the Daubechies coefficients (Refs. 8 and 9) are used to generate these wavelets. Note that *db2*, which is used in this analysis, spans a bit less than 3 units over the x-axis. Daubechies' family of wavelets satisfies two crucial requirements: orthogonality of local basis functions, and second or higher-order accuracy, depending on the dilation expression adopted (Ref. 10).

In order to use the wavelet transformation in practical applications, a way to define a discrete version of the transformation shown in Equation 7 must be found. For this purpose, the range of the independent variable x is limited to the unit interval [0,1), and a wavelet series expansion performed over that interval (Ref. 11). A complication arises since some of the wavelets $W(2^j x-k)$ overlap the edges of the interval. For this reason, it is convenient to assume that $f(x)$ is one period of a periodic signal exactly repeated in the adjacent unit intervals. Note that with the D4 wavelet family $W(x)$ spans almost three units. Over the interval [0,1) there are contributions from three bases: from the first third of $W(x)$, from the middle third of $W(x+1)$, and from the last third of $W(x+2)$. This is equivalent to $W(x)$ being wrapped around the unit interval. Thus the wavelet expansion of $f(x)$ in the [0,1) interval can be written as:

$$f(x) = a_0\varphi(x) + a_1 W(x) + \begin{bmatrix} a_2 & a_3 \end{bmatrix}\begin{bmatrix} W(2x) \\ W(2x-1) \end{bmatrix} + \begin{bmatrix} a_4 & a_5 & a_6 & a_7 \end{bmatrix}\begin{bmatrix} W(4x) \\ W(4x-1) \\ W(4x-2) \\ W(4x-3) \end{bmatrix} + \ldots$$

$$+ a_{2^j+k} W(2^j x - k) + \ldots \tag{7}$$

The coefficients a_1, a_2, a_3, a_4, ... give the amplitudes of the contributing wavelets (after wrapping) to one cycle of the periodic function in the [0,1) interval. Because of orthogonality conditions, the general wavelet transform coefficients can be found by

$$a_{2^j+k} = 2^j \int_0^1 f(x) W(2^j x - k) dx, \qquad a_0 = \int_0^1 f(x)\varphi(x) dx \tag{8}$$

The discrete wavelet transform (DWT) is an algorithm for computing Equations 7 and 8 when $f(x)$ is sampled at equally spaced intervals over [0,1). As stated before, it is assumed here that $f(x)$ is one period of a periodic signal and that the scaling and wavelet functions wrap around the interval [0,1). A remarkable feature of the DWT algorithm is that there is no need to compute $\varphi(x)$ or $W(2^j x-k)$ explicitly. A MATLAB implementation of this DWT algorithm, found in Appendix 7 of Ref. 11, was discovered by Mallat, and is often referred by as the *Mallat's pyramid algorithm*.

DWT-Based Extraction of the Markov Parameters

The DWT method starts with the convolution integral,

$$y(t_n) = \int_{-\infty}^{t_n} h(t_n - \tau) u(\tau) d\tau = \int_0^1 h(\theta) u(t_n - \theta) d\theta \tag{9}$$

Note that $h(\theta)$ is the temporal impulse response function. The impulse response function is expanded in terms of the wavelet basis functions for the entire time interval, $0 \le \theta < 1$;

$$h(\theta) = h_0^{DWT} + \sum_j \sum_k h_{2^j+k}^{DWT} W(2^j \theta + k) \tag{10}$$

where the h^{DWT} terms are the expansion coefficients. For the DWT characterization of $u(t_n-\theta)$, first $u(\theta)$ is reversed in time to obtain $u(-\theta)$, then it is shifted toward the positive time axis by an amount t_n. Following this, $u(t_n-\theta)$ can be expressed as

$$u(tn - \theta) = u_0^{DWT} + \sum_i \sum_j u_{2^j+k}^{DWT} W(2^j \theta + k) \tag{11}$$

Substituting Equations 10 and 11 into Equation 9, and making use of the orthogonality conditions, yields the following formula (Ref. 11):

$$y(t_n) = h^{DWT} u^{DWT}(t_n) \tag{12}$$

For the entire data sample, the inputs and outputs are arranged in the form

$$Y = h^{DWT} U^{DWT} \tag{13}$$

Solving for h^{DWT} (Ref. 9),

$$h^{DWT} = Y\, U^{DWT^T} (U^{DWT}\, U^{DWT^T})^{-1} \tag{14}$$

The desired temporal impulse response data is finally obtained by taking the inverse wavelet transform of h^{DWT}. (See Ref. 11 for details on how to implement the inverse wavelet transform.)

$$h(t) = IDWT(h^{DWT}) \tag{15}$$

ANALYSIS EXAMPLE

Aircraft Model Description

During developmental flight testing of a modern fighter aircraft, an unacceptable 5.0 to 6.0 Hz LCO was experienced at high speed, low altitude flight with certain store configurations (Ref. 12). The approaches investigated to suppress the limit cycle included variations in store orientation, wing control surface biasing, and active oscillation suppression. Changes in store orientation and biasing techniques did not sufficiently reduce the problem, so various active suppression techniques were evaluated. The successful active oscillation control approach used a passive band pass filter to command aileron deflections with gain and phase set by flight control system lateral acceleration input signals. This system was incorporated into the production aircraft using existing flight control system components.

Under a subcontract to STI, The Boeing Company provided aeroservoelastic models of this fighter aircraft (see also Ref. 13). The aircraft was configured with full 330-gallon tanks on the inboard pylons and MK-84s (i.e., 2,000 lb bombs) on the outboard pylons, a configuration that produced LCO in flight. The models were formulated at twelve flight conditions, below, at, and above the aircraft's flutter boundary, as identified in Figure 1. The lateral-directional model was provided in the form of ABCD state space matrices for the rigid body airframe, aeroservoelastic (ASE) dynamics, rigid body control system, ASE control, plant input time delay, zero order hold, and sensors. Inputs to the model are the stick and rudder positions, and outputs consist of the rigid body dynamics, flexible dynamics, and accelerator data at various locations on the aircraft. A block diagram of the model is shown in Figure 2. The ASE dynamics and the active oscillation controller (AOC) can be turned on or off. A block diagram and Bode frequency response of the band pass filter implementation of the AOC is shown in Figure 3. As described in Ref. 13 the controller is activated as a function of Mach number and altitude, and only for the specific set of stores where LCO is known to occur.

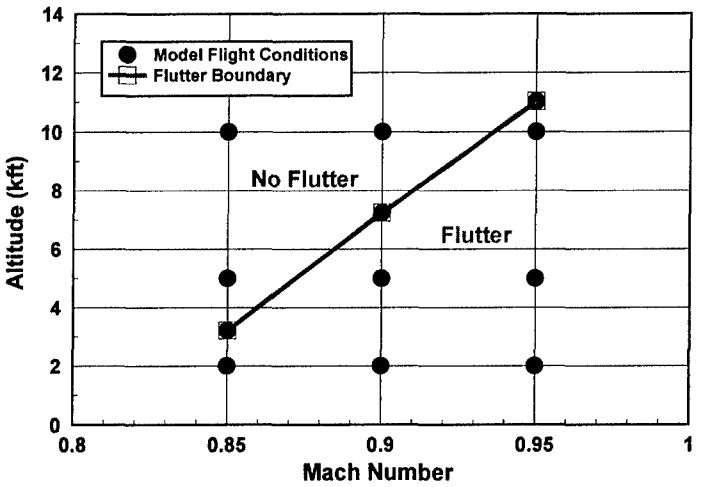

Figure 1. Aeroservoelastic Model Flight Conditions

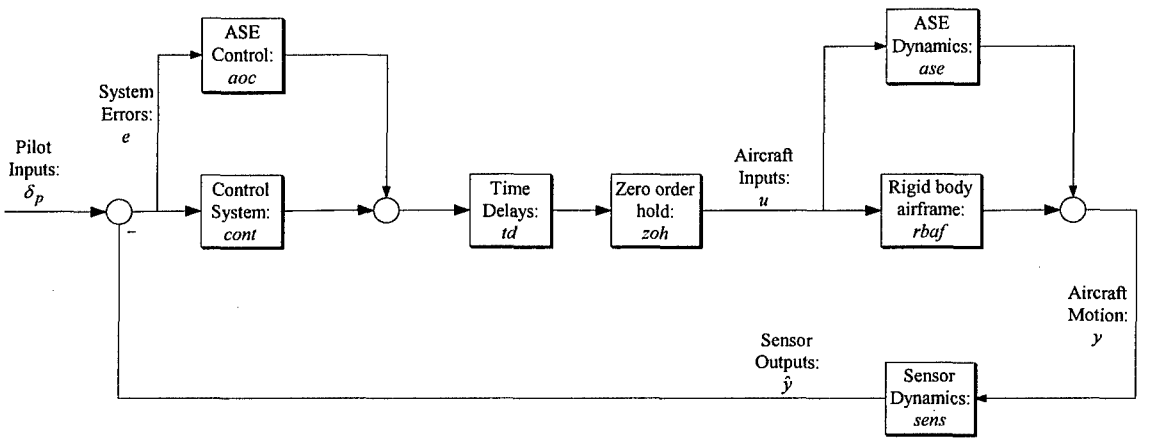

Pilot Inputs: δ_p =		
1	Latstk	in
2	Pedal	lbs
3	0	
4	0	
5	0	
6	0	
7	0	
8	0	
9	0	

Sensor Outputs: $\hat{y}$ =		
1	0	
2	0	
3	Beta	deg
4	Roll	deg
5	Yaw	deg
6	Roll rate	deg/sec
7	Yaw rate	deg/sec
8	Ny rbcl	g
9	Ny aoc	g

Aircraft Inputs: u =		
1	Dif LEF cmd	deg
2	Dif TEF cmd	deg
3	Dif Ail cmd	deg
4	Dif Stab cmd	deg
5	Coll Rudder cmd	deg

Aircraft Motion: y =		
1	Beta	rad
2	Phi	rad
3	Psi	rad
4	Roll Rate	rps
5	Yaw Rate	rps
6	Ny rbcl	g
7	Ny aoc	g

(ASE Data)		
8,9	Ny fwd,aft	g
10,11	P,R fwd	rps
12,13	P,R aft	rps
14-16	Nz wing row 1 fwd,mid,aft	g
17-19	Nz wing row 2 fwd,mid,aft	g
20-22	Nz wing row 3 fwd,mid,aft	g
23-26	Nz wing row 4 fwd,mid,aft	g
26,27	Nz inbrd store fwd,aft	g
28,29	Nz outbrd store fwd,aft	g
30,31	Nz tip missile fwd,aft	g

Figure 2. Modern Fighter Lateral Axis Rigid Body and ASE Dynamics, with Rigid and AOC Control

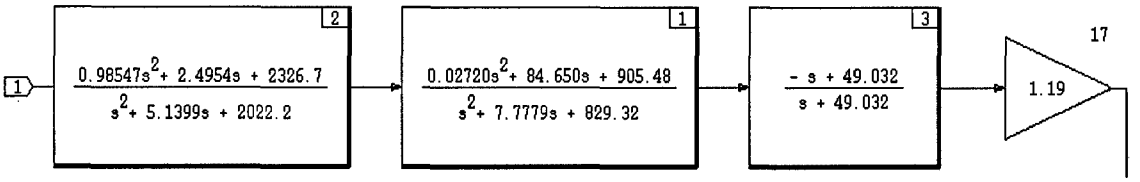

a) Filter Block Diagram: Input – n_{y_AOC} (g), Output – δ_{a_c} (deg)

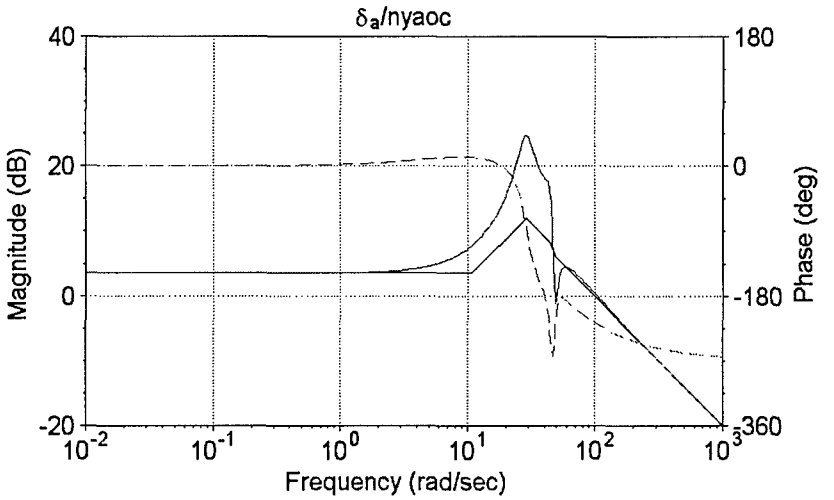

b) AOC Frequency Response

Figure 3. Active Oscillation Controller

Assessment of WERA Identification

Figure 4a compares the frequency responses of the actual and estimated aeroservoelastic dynamics for the Mach 0.9, 10,000 ft altitude flight condition, showing excellent agreement in both magnitude and phase. The discrete wavelet transform is used to compute the impulse response (Markov parameters) of the estimated system, which is used in the Eigensystem Realization Algorithm (ERA) method (Ref. 14) to compute the discretized state-space matrices. Accurate system identification thus rests in large part on the quality of the impulse response estimate. In Figure 4b the actual and estimated impulse responses are practically indistinguishable from one another; however, there may be cases where the estimated impulse response degrades significantly toward the tail of the impulse data-window (due to noise, precision error, etc.). This degradation typically is seen as a rapid oscillatory divergence in amplitude. Normally the impulse response sees a maximum peaking shortly after start-up, followed by decaying oscillations that taper towards zero or resonate with low-amplitude. In order to ensure proper choice of impulse length, the impulse response is divided into time bins following the maximum start-up peak, and the standard deviation of these bins is computed. If the standard deviation of a bin is greater than the one preceding it, the impulse response is terminated at the preceding bin. This procedure systematizes window-length selection, and ensures maximum use of available data.

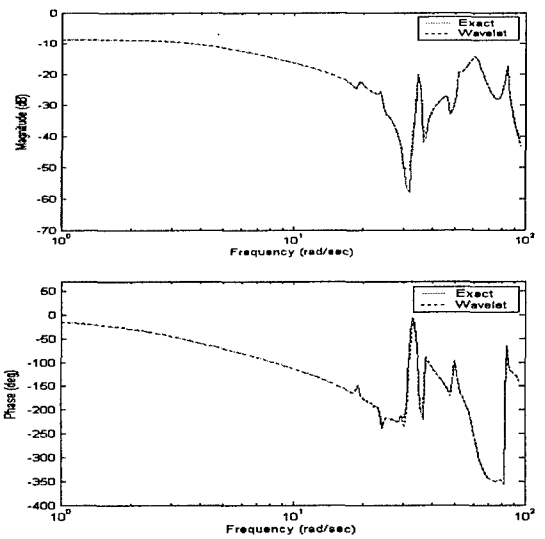

a) Frequency Response

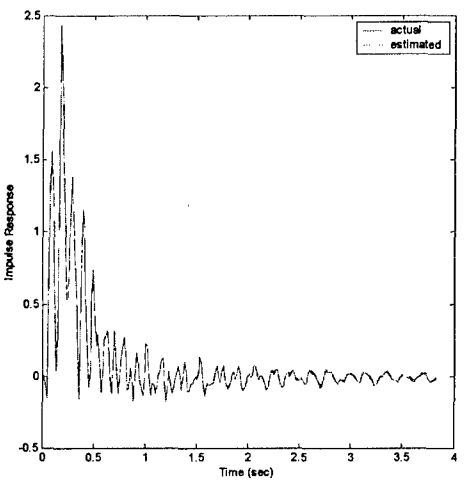

b) Impulse Response

Figure 4. Model Estimates and Comparisons for Mach = 0.9, Altitude = 10,000 ft Flight Condition

In Equation 16 the *ABCD* matrices identified with the ERA method are transformed to modal coordinates, and Equation 17 computes the modal time history for the i^{th} mode. The modal pulse response used in the identification is computed with Equation 18, where $R\Sigma S^T$ are the singular value decomposition matrices of the Hankel matrix whose elements are the impulse responses. The dot product between Equations 17 and 18 is defined as the Modal Amplitude Coherence (MAC), shown in Equation 19. The MAC is an important metric of confidence that compares the modal time history computed two different ways – if the two methods yield a close match for a particular mode, there is high likelihood that the mode has been correctly identified. Figure 5 shows the MACs for this example to be essentially unity at all modes, which is consistent with the excellent fits seen in Figure 4a and b.

$$\hat{A} = \hat{\Psi}\hat{\Lambda}\hat{\Psi}^{-1} \qquad \hat{A}_m = \Lambda$$

$$\hat{B}_m = \hat{\Psi}^{-1}\hat{B} \qquad C_m = \hat{C}\hat{\Psi} \qquad \hat{D}_m = \hat{D}$$

$$\hat{q}_i = \left[\hat{b}_i \quad \lambda_i \hat{b}_i \quad \lambda_i^2 \hat{b}_i \quad \cdots \quad \lambda_i^{l-2} \hat{b}_i\right] \tag{16}$$

$$\bar{Q} = \hat{\Psi}^{-1} \Sigma_n^{1/2} S_n^T \tag{17}$$

$$MAC_i = \frac{\left|\bar{q}_i \hat{q}_i^*\right|}{\left|\bar{q}_i \bar{q}^*{}_i\right| \left|\hat{q}_i \hat{q}_i^*\right|} \tag{18}$$

(19)

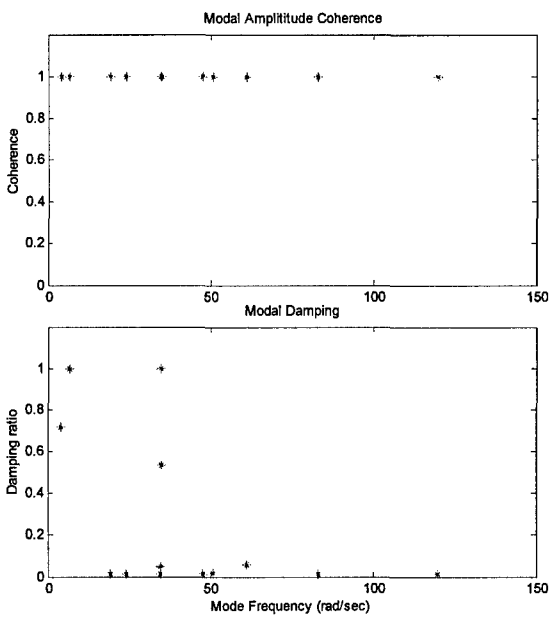

Figure 5. Mode Amplitude Coherence and Damping for the Figure 4 Model Estimates

A metric that indicates the relevance of the mode identified is given in Equation 20, called the Mode Singular Value (MSV). This is a measure of the contribution of each identified mode to the identified pulse response history – if a pole is nearly cancelled by a zero one would expect the MSV at that mode to be very small. While it is not feasible for an identification algorithm to compute all modes of a system, a system has *effectively* been estimated when actual modes corresponding to high MSVs are closely aligned with estimated modes that exhibit similarly high MSVs. The algorithm searches for the closest estimated mode to every actual mode (using natural frequency and damping as distances). The absolute value of the MSV difference between the actual and estimate is then computed, shown in Figure 3d where for clarity only damping values less than 0.1 are shown. If more than one actual mode is in close proximity to an estimated mode, the actual mode with the highest MSV is differenced with the estimate. The MSVs of the remaining actual modes that have not been paired with estimated modes are simply plotted by themselves. A well-estimated system would thus exhibit MSV differences and stand-alone values that are all approximately the same order of magnitude, indicating that the actual modes not identified were comparatively negligible. This in fact is the case in Figure 3d.

$$MSV_i = \sqrt{\left|\hat{c}_i\right|\left(1+\left|\hat{\lambda}_i\right|+\left|\hat{\lambda}_i^2\right|+\cdots+\left|\hat{\lambda}_i^{l-2}\right|\right)\left|\hat{b}_i\right|} \tag{20}$$

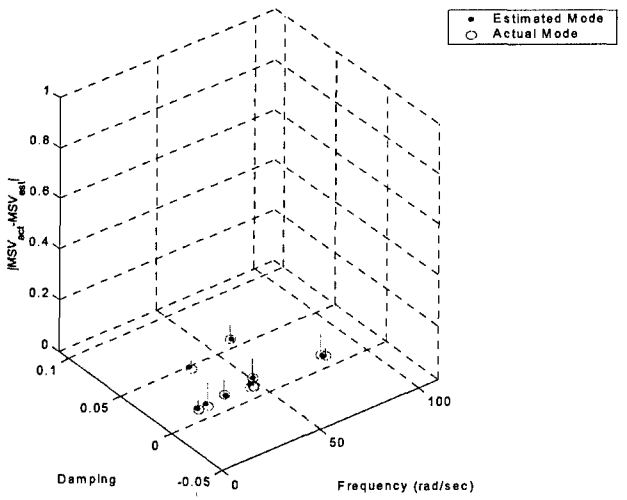

Figure 6. Mode Singular Value Differences for the Figure 4 Model Estimates

The MSV metric defined above is for the identified, digital system. We have explored the use of equivalent metrics for analog systems. This is important because our model is analog, and high order (greater than 100), and numerically it is better to compute the MSV using the analog model. Define the following analog system and the ZOH-equivalent digital system:

$$\text{Analog system: } \begin{cases} \dot{x} = Ax + Bu \\ y = Cx + Du \end{cases} \tag{21}$$

$$\text{Eigenstructure: } A = X\Lambda X^{-1},\ X = \left[x_1 \cdots x_n\right],\ \Lambda = \text{diag}(\lambda_1 \cdots \lambda_n),\ X^{-T} = \left[y_1 \cdots y_n\right] \tag{22}$$

$$\text{Residue of mode } \lambda_i = \sigma_i + j\omega_i \ :\ R_i = Cx_i y_i^T B \tag{23}$$

$$\text{analog MSV}_i = \frac{1}{|\sigma_i|}\sigma_{\max}(R_i) \tag{24}$$

$$\text{ZOH-equivalent digital system: } \begin{cases} x(k+1) = \Phi x + \Gamma u \\ y = Cx + Du \end{cases},\ \text{where } \Phi = e^{AT},\ \Gamma = \int_0^T e^{A\tau} B d\tau \tag{25}$$

$$\text{Eigenstructure: } \Phi = Xe^{\Lambda T}X^{-1},\ X, \Lambda, X^{-1} = \text{same as for analog system} \tag{26}$$

$$\text{Residue of mode } z_i = e^{\lambda_i T} \ :\ S_i = Cx_i y_i^T \Gamma$$

(27)

$$\text{digital MSV}_i = \frac{1}{1-|z_i|}\sigma_{\max}(S_i)$$

(28)

The new result is that the residues and modal singular values are related by:

$$S_i = R_i\frac{1-z_i}{\lambda_i} \quad , \quad \text{digital MSV}_i = \text{analog MSV}_i \times \left|\frac{\sigma_i}{\lambda_i}\right| \times \frac{|1-z_i|}{1-|z_i|}$$

(29)

Beyond the Flutter Boundary Analysis

Figure 7 shows results using Flight Condition 6 with the Oscillation Controller activated. When the Oscillation Controller is deactivated, an unstable pole is identified at approximately 34 rad/sec, which agrees with the model for this flight condition (Figure 8). Note the divergence of amplitude in the Figure 8 time histories.

CONCLUSIONS

A method for rapid, on-line identification of aeroservoelastic systems has been developed that employs discrete wavelet transforms. The wavelet transforms compute the system impulse response, which is then used in the Eigensystem Realization Algorithm (ERA) method to generate the discretized state-space matrices. The method was demonstrated using an aeroservoelastic model of a modern military fighter. Modal Amplitude Coherence and Mode Singular Value metrics were defined. Excellent agreement was observed between the aeroservoelastic model and the estimated system.

ACKNOWLEDGEMENTS

The work described herein was conducted as part of a Phase II Small Business Innovation Research (SBIR) program for the Air Force Flight Test Center (AFFTC) to improve flutter flight test techniques in the presence of an automatic flutter suppression system. The aircraft model used in the analysis was provided by the Boeing Company, St. Louis, MO under contract to Systems Technology, Inc. as part of this program. Mr. Rudy Yurkovich led the Boeing effort.

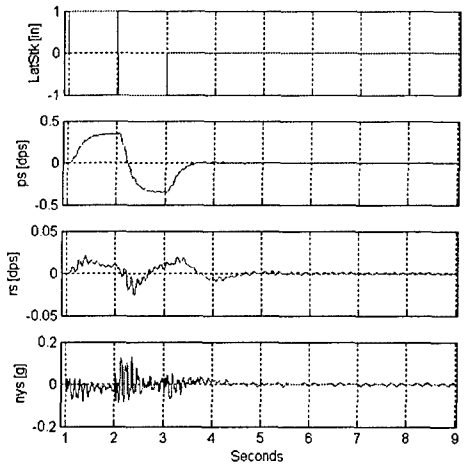

a) Lateral Stick Input and Output Time Histories

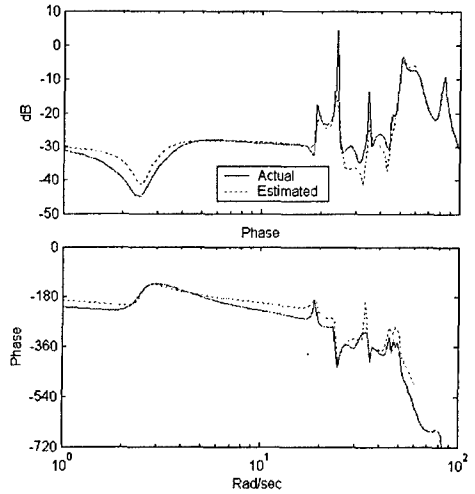

b) Frequency Response Comparison

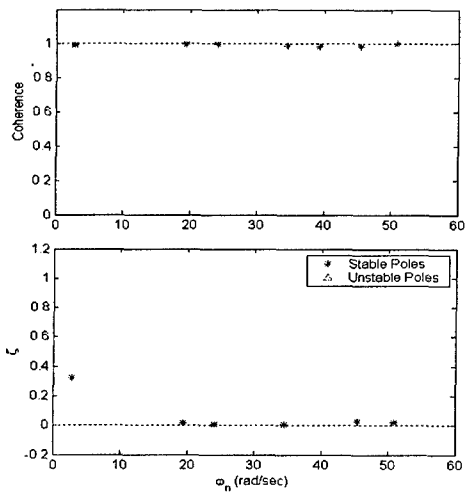

c) Mode Amplitude Coherence and Damping

Figure 7. Model Estimates and Comparisons for Mach = 0.9, Altitude = 5,000 ft Flight Condition AOC On

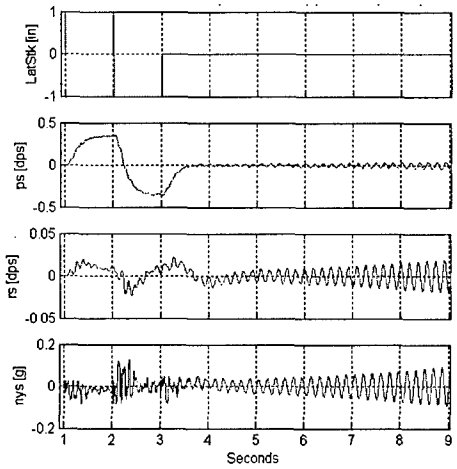

a) Lateral Stick Input and Output Time Histories

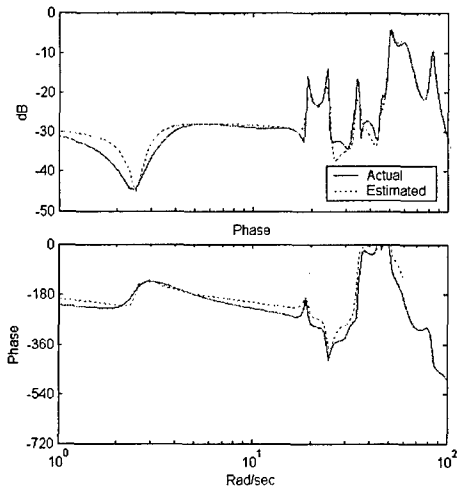

b) Frequency Response Comparison

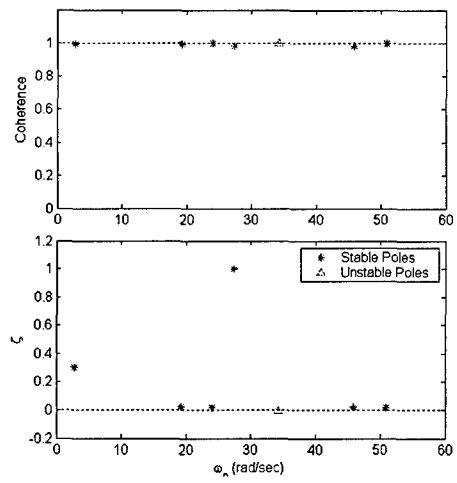

c) Mode Amplitude Coherence and Damping

Figure 8. Model Estimates and Comparisons for Mach = 0.9, Altitude = 5,000 ft Flight Condition AOC Off

REFERENCES

1. Tanner, Roger, MAJ USAF, and Jerry M. Ogden, "F-16 Active Flutter Suppression System," *42nd Symposium of the Society of Experimental Test Pilots*, Beverly Hills, CA, 24-26 Sep. 1998.
2. Farhat, C., C. Harris, and D. J. Rixen, "Expanding a Flutter Envelope Using Accelerated Flight Data: Application to an F-16 Fighter Configuration," AIAA 2000-1702 presented at the *41st AIAA/ASME/ASCE/AHS/ASC SDM*, Atlanta, GA, 3 – 6 April 2000.
3. Geuzaine, P., G. Brown, and C. Farhat, "Three-Field Based Nonlinear Aeroelastic Simulation Technology: Status and Application to the Flutter Analysis of an F-16 Configuration," AIAA 2002-0870 presented at the *40th Aerospace Sciences Meeting and Exhibit*, Reno, NV, 14-17 Jan. 2002.
4. Bendat J. S., and A. G. Piersol, Engineering Applications of Correlation and Spectral Analysis, John Wiley and Sons, New York, N.Y., 1993.
5. Schwartz, R. J., Linear Systems, McGraw-Hill, New York, N.Y., 1985.
6. Newland, D.E., "Wavelet Analysis of Vibration, Part 1: Theory," *ASME Journal of Vibration and Acoustics*, Vol. 116, October 1994, pp. 409-416
7. Strang, G., and T. Nguyen, Wavelets and Filter Banks, Wellesley-Cambridge Press, 1997.
8. Daubechies, I., "Orthonormal Bases of Compactly Supported Wavelets," *Commun. Pure Appl. Math.*, Vol. 41, 1988, pp. 909-996.
9. Daubechies, I., "The Wavelet Transform, Time-Frequency Localization and Signal Analysis," *IEEE transactions in Information Theory*, Vol. 36, 1990, pp. 961-1005.
10. Robertson, A. N., K. C. Park, and K. F. Alvin, "Extraction of Impulse Response Data via Wavelet Transform for Structural System Identification", *ASME Journal of Vibration and Acoustics*, Vol. 120, 1993, pp. 252-260.
11. Newland, D.E., Random Vibrations, Spectral & Wavelets Analysis, 3rd edition, Longman Scientific and Technical, Essex, England, 1988.
12. Trame, L. W., L. E. Williams, and R. N. Yurkovich, "Active Aeroelastic Oscillation Control of the F/A-18 Aircraft," AIAA Paper No. 85-1858 presented at the *AIAA Guidance, Navigation and Control Conference*, Snowmass, CO, 19 to 21 Aug. 1985.
13. Goodman, C., M. Hood, E. Reichenbach, and R. Yurkovich, "An Analysis of the F/A-18C/D Limiti Cycle Oscillation Solution," AIAA Paper No. 2003-1424 presented at the *44th Structures, Structural Dynamics and Materials Conference*, Norfolk, VA, 7-10 April 2003.
14. Juang, J., Applied System Identification, Prentice Hall, 1994.